Measuring Component Contributions to the Dynamic Modulus in Miscible Polymer Blends

Jeffrey A. Zawada[†] and Gerald G. Fuller*

Department of Chemical Engineering, Stanford University, Stanford, California 94305-5025

Ralph H. Colby

Imaging Research and Advanced Development, Eastman Kodak Company, Rochester, New York 14650-2109

Lewis J. Fetters

Corporate Research—Science Laboratories, Exxon Research and Engineering Company, Annandale, New Jersey 08801

Jacques Roovers

Institute for Environmental Chemistry, National Research Council of Canada, Ottawa, Ontario, Canada K1A 0R6

Received October 22, 1993; Revised Manuscript Received August 5, 1994[⊕]

ABSTRACT: A novel approach to investigating the rheology of miscible polymer blends is described based on complementary infrared polarimetry and mechanical rheometry measurements. The method provides a means by which the blend dynamic modulus $G^*(\omega)$ may be separated into the individiual contributions due to each of the blend components. This separation is made possible by converting the observables of dynamic infrared 1,3-dichroism and birefringence experiments to those of dynamic shear stress experiments through the use of constitutive relations and the application of the stress-optic rule. The approach is extended to cover blend systems which exhibit orientational coupling, an effect which influences the optical anisotropies but does not contribute to the state of stress. Validity of the analysis technique is demonstrated by studying highly entangled miscible blends of 1,4-polyisoprene, PI (M_w = 75 000), and 1,2-polybutadiene, 1,2-PB (M_w = 204 000), containing a fraction of deuterium-labeled PI chains (M_w = 90 000). Orientational coupling in this blend is observed and is found to be characterized by a coupling coefficient $\epsilon = 0.35 \pm 0.05$.

1.0. Introduction

The rheological behavior of viscoelastic polymeric systems is a fundamental concern in the processing and often the end use of such materials. In general, however, a universal characterization of the stress–strain behavior for a given polymer system subjected to an arbitrary deformation history is unrealistic even for simple geometries, as the stress tensor is typically a complicated, nonlinear function of deformation. Consequently, rheological characterization is often restricted to the limiting case of small deformation gradients, for which the stress and rate of strain tensor become linearly related.[1,2] The most popular means for characterizing polymer viscoelasticity in this limit is the rheometric measurement of shear stress induced by simple shear deformation. For such experiments, the linear viscoelastic constitutive relation between the shear stress $\sigma_{12}(t)$ and the shear strain $\gamma(t)$ may be written as

$$\sigma_{12}(t) = \int_{-\infty}^{t} G(t-s) \frac{\partial}{\partial s}\gamma(s)\, ds \qquad (1)$$

where the relaxation modulus $G(t)$ contains the rheologically significant information about the material. Typically, it is the dynamic modulus $G^*(\omega)$, related to $G(t)$ by Fourier transformation,[1] which is experimentally measured. As with $G(t)$, analysis of $G^*(\omega)$ provides insight to the molecular relaxation dynamics underlying the viscoelastic behavior.

In the case of a multicomponent system (such as a homopolymer melt of bidisperse molecular weight or a blend of two different polymer species), the standard assumption that the total stress is simply the sum of the stress borne by each of the components is made. Thus, the dynamic modulus of a binary mixture of polymer components A and B may be broken down as follows:

$$G^*(\omega) = G_A^*(\omega) + G_B^*(\omega) \qquad (2)$$

It is important to bear in mind that G_A^* and G_B^* are not necessarily related in a simple manner to the pure component moduli. This is evident even for the simple case of bidisperse homopolymer blends (i.e., A and B differ only in molecular weight). According to the pure reptation model,[3] for a bidisperse linear homopolymer system, G_A^* and G_B^* are given by their pure component values weighted according to their respective volume fraction in the blend (i.e., $G_K^* = \phi_K G_K^*{}_0$). However, this prediction is inconsistent with numerous experiments,[4-8] suggesting that G_A^* and G_B^* must vary with blend composition in a more complicated fashion (an effect which is attributed to additional and/or modified modes of relaxation available in the presence of the second component).

To gain a thorough understanding of the rheology of a multicomponent system, recovery of the component contributions to G^* would clearly be rewarding. With explicit knowledge of each component's G^* contribution, the effects of blending on the rheology of each component could then be directly monitored. Unfortunately, conventional rheometry alone cannot accomplish this since direct mechanical measurements of stress only yield observations of bulk behavior. In this report we describe

* To whom correspondence should be addressed.
[†] Present address: Eastman Chemical Co., Kingsport, TN 37662.
[⊕] Abstract published in *Advance ACS Abstracts*, September 15, 1994.

0024-9297/94/2227-6851$04.50/0

a novel method by which the dynamic modulus of a binary miscible polymer blend may, in fact, be separated into blend component contributions by complementing mechanical rheometry experiments with dynamic infrared dichroism and birefringence measurements. Previous researchers have combined results of such techniques in related rheological studies. Osaki et al.[9,10] have applied mechanical rheometry and birefringence to block copolymers in solution subjected to a step shear, and Monnerie and co-workers[11,12] have used infrared dichroism and birefringence to study orientation in blends under uniaxial extension. The current work, however, is unique in that it provides a means for recovering the component contributions to the dynamic modulus, which can be used to gain greater insight to the stress contributions and relaxation dynamics in blends.

Validity of the current technique is demonstrated with miscible blends of narrow molecular weight distribution 1,4-polyisoprene (PI) and atactic 1,2-polybutadiene (1,2-PB). This blend system is attractive from an experimental standpoint since these polymers have disparate stress-optic coefficients, facilitating the distinction of each component's contribution to birefringence. Furthermore, due to the similarity in chemical constitution of the species and the absence of specific interactions between the species (demonstrated by FTIR[13] and SANS[14]), bond polarizabilities of the components and hence their stress-optic coefficients are not expected to vary upon blending. A detailed investigation of the effects of blending upon the component contributions to the bulk rheology in this particular miscible blend system is discussed in the companion paper.[15] Here we focus on developing the technique and demonstrating its feasibility.

2.0. Relating Optical Anisotropies to Dynamic Moduli

Recovery of blend component contributions to the dynamic modulus relies on converting the observables of dynamic rheo-optical experiments to those of dynamic shear experiments. For the experimental approach presented here, this process involves utilizing constitutive relationships between the normal stress differences and the shear stress and invoking the stress-optic rule in a form applicable to miscible polymer blends. In the following two sections the method for the separation of G^* into blend component contributions using these steps is developed. The approach is then extended to cover blend systems which exhibit appreciable orientational coupling, an effect which influences the optical anisotropies but does not contribute to the state of stress.

2.1. Constitutive Relationship between Shear and Normal Stresses. In the polarimetry experiments described here with transmission along the 2-axis (see Figure 1), birefringence and dichroism are sensitive to molecular orientation projected onto the 1,3-plane. With the deformation imposed along the 1-axis and the velocity gradient in the 2-direction, such measurements are related to the third normal stress difference,[16] $N_3 = \sigma_{11} - \sigma_{33}$. This geometry permits the use of a short optical path length (desirable in measuring birefringence, especially in melts) without introducing adverse end effects to the polarimetry measurements. In contrast, the shear stress measured by dynamic mechanical rheometry arises from the segmental orientation projected onto the 1,2-plane. Since the two techniques used in this work are sensitive to different elements of the stress tensor (or equivalently to different projections of the segmental orientation), a means of relating the N_3 and σ_{12} responses in necessary to compare the results of the optical and mechanical experiments.

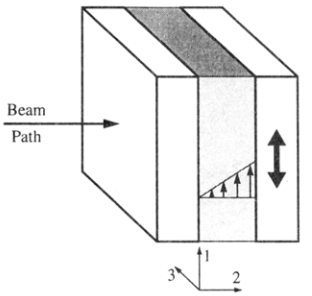

Figure 1. Flow cell geometry used in the rheo-optical experiments. The sample (shaded region) is bound between parallel CaF_2 windows, whose surface normals lie in the 2-direction. Shear is applied by translating the rear window in the 1-direction, and the optical beam is transmitted along the 2-axis.

Such relationships applied to the case of oscillatory shear in the limit of linear viscoelasticity are developed here.

According to linear viscoelasticity, for a small-amplitude sinusoidal shear strain of maximum amplitude γ° and frequency ω (i.e., $\gamma(t) = \gamma^\circ \sin \omega t$), viscoelastic liquids manifest normal stress difference and shear stress responses of fundamentally different transient forms. More familiar is the shear stress response, which exhibits a sinusoidal time dependence having the same frequency as the applied strain but with shifted phases. In contrast, although each of the three normal stress differences ($N_1 = \sigma_{11} - \sigma_{22}$, $N_2 = \sigma_{22} - \sigma_{33}$, $N_3 = N_1 + N_2$) behaves as a phase-shifted sinusoid like the shear stress, for symmetry reasons the N_j responses (where $j = 1$–3) oscillate at twice the applied strain frequency and in addition vary about a nonzero displacement. The stress–strain relationships[1] for σ_{12} and N_j are concisely expressed in terms of viscoelastic material functions, G', G'', ψ_j', ψ_j'', ψ_j^{d}:

$$\sigma_{12}(t) = \gamma^\circ[G'(\omega) \sin \omega t + G''(\omega) \cos \omega t] \tag{3}$$

$$N_j(t) = (\gamma^\circ\omega)^2[\psi_j^{\mathrm{d}}(\omega) + \psi_j'(\omega) \cos 2\omega t + \psi_j''(\omega) \sin 2\omega t] \tag{4}$$

The complex dynamic modulus is given by $G^*(\omega) = G'(\omega) + iG''(\omega)$, the complex normal stress difference coefficients are expressed as $\psi_j^*(\omega) = \psi_j'(\omega) - i\psi_j''(\omega)$, and the normal stress difference displacement coefficients are $\psi_j^{\mathrm{d}}(\omega)$. Dynamic mechanical rheometry provides $G^*(\omega)$ for the bulk, while the optical measurements are related to the component contributions to $\psi_3^*(\omega)$ and $\psi_3^{\mathrm{d}}(\omega)$. Due to an inherent baseline drift in the optical technique, there is significant uncertainty in the determination of ψ_j^{d}, and since ψ_j^{d} is not essential for our purposes, we restrict our attention here to ψ_3^*.

For linear viscoelastic response, the following relations hold:[1,17]

$$\omega^2\psi_1^*(\omega) = -G^*(\omega) + \frac{1}{2}G^*(2\omega) \tag{5}$$

$$\psi_3^*(\omega) = \alpha\psi_1^*(\omega) \tag{6}$$

where $\alpha \equiv N_3/N_1 = 1 + (N_2/N_1)$ is a constant whose value depends on additional constitutive assumptions. Several experimental reports support the validity of (5) and (6) for concentrated polymer solutions and entangled melts in oscillatory shear. These include the work of Gao et al.,[17] who measured dynamic viscosity along with first and second normal stress differences in concentrated polystyrene solutions, Kornfield et al.,[8,18] who used 1,3-birefringence, IR dichroism, and stress rheometry of poly(ethylenepropylene) melts, and, more recently, Kannan and Kornfield[19] using 1,2- and 1,3-birefringence along

with simultaneous shear stress measurements on poly(ethylenepropylene) and polyisoprene melts. The proportionality between the normal stress differences predicted by (6) has also been confirmed by birefringence and shear stress measurements on entangled polystyrene solutions subjected to step shear strains[20] and by steady shear measurements of N_1 and N_2 on low-density polyethylene melts.[21] Results on the pure components in this study provide further verification of these relationships.

Substituting (6) into (5) and expressing the real and imaginary parts separately yield

$$-\omega^2\psi_3'(\omega) = \alpha\left[G'(\omega) - \frac{1}{2}G'(2\omega)\right] \quad (7)$$

$$\omega^2\psi_3''(\omega) = \alpha\left[G''(\omega) - \frac{1}{2}G''(2\omega)\right] \quad (8)$$

These relations have been previously appreciated and applied to make comparisons between mechanically measured G^* and optically measured ψ_3^* by calculating a predicted ψ_3^* from the mechanical G^* data.[8,18,19] However, the reverse calculation (i.e., converting the optical ψ_3^* results into G^*) has not been previously reported. Equations of such form may be inverted by iterative substitution, providing expressions for G' and G'' in terms of ψ_3' and ψ_3'':

$$G'(\omega) = -\frac{1}{\alpha}\sum_{m=0}^{\infty}\frac{1}{2^m}[(2^m\omega)^2\psi_3'(2^m\omega)] \quad (9)$$

$$G''(\omega) = \frac{1}{\alpha}\sum_{m=0}^{\infty}\frac{1}{2^m}[(2^m\omega)^2\psi_3''(2^m\omega)] \quad (10)$$

The quantities in square brackets are simply $\omega^2\psi_3^*$ values at frequency multiples of 2. For entangled linear polymer melts of narrow molecular weight distribution the bracketed quantity in (9) approaches a finite plateau at high ω (large m), while for (10) this factor passes through a maximum and then decreases at high ω. As a result, provided that the available data to extend to high frequencies (i.e., beyond the terminal relaxation regions of both blend components), a reliable evaluation of G' and G'' may be realized with these expressions even for ψ_3^* data over a finite ω-range due to the rapid decay of the $1/2^m$ coefficient with increasing m and the bounded values of the quantities in square brackets. For an experimental ω-range spanning several decades, the use of partial sums in (9) and (10) leads to less than 1% error over most of the ω-range, except at the very highest frequencies (since the number of terms available for summing diminishes as the highest experimental frequency limit is approached). To improve the accuracy of the calculated G^* at high frequencies, a correction factor of $2^n/(2^n - 1)$ (where n is the number of terms included in the partial sum) is introduced to the analysis here to account for series truncation. This factor assumes the neglected terms are of the same order as the included terms, and it should be noted that this factor exceeds 1.07 only for calculations at the three highest values in a given experimental frequency range (reflecting the rapid convergence of the summations in (9) and (10)). Comparison of results on the pure components with and without the correction factor confirms that in practice the correction does indeed improve the calculation of G^* from ψ_3^*.

2.2. Stress-Optic Relationship. Equations 9 and 10 provide the means of transforming third normal stress difference measurements into shear stress counterparts. Because the third normal stress difference is probed indirectly via optical anisotropies, further relations are needed to equate the experimental optical observables to the actual stress experienced by the material. Anisotropic optical properties are associated with the deviatoric part of the refractive index tensor: $n_{ij} = \hat{n}_{ij} - {}^1/_3\, n\delta_{ij}$, where $\hat{n}_{ij}$ is the full refractive index tensor and n is the isotropic part. In general, n_{ij} is a complex tensor ($n_{ij} = n_{ij}' + in_{ij}''$), whose real part, n_{ij}', characterizes the retardation of light by the material and whose imaginary part, n_{ij}'', characterizes the attenuation of light by the material. The specific anisotropies measured by the dynamic optical experiments here are 1,3-birefringence, $\Delta n' = n_{11}' - n_{33}'$, and 1,3-dichroism, $\Delta n'' = n_{11}'' - n_{33}''$, whose transient responses are analogous to the N_3 response:

$$\Delta n'(t) = (\gamma^\circ\omega)^2[\psi_{3,\mathrm{Bi}}{}^{\mathrm{d}}(\omega) + \psi_{3,\mathrm{Bi}}'(\omega)\cos 2\omega t + \psi_{3,\mathrm{Bi}}''(\omega)\sin 2\omega t] \quad (11)$$

$$\Delta n''(t) = (\gamma^\circ\omega)^2[\psi_{3,\mathrm{Di}}{}^{\mathrm{d}}(\omega) + \psi_{3,\mathrm{Di}}'(\omega)\cos 2\,\omega t + \psi_{3,\mathrm{Di}}''(\omega)\sin 2\,\omega t] \quad (12)$$

For the reason mentioned previously we restrict our attention here to $\psi_{3,\mathrm{Bi}}'$, $\psi_{3,\mathrm{Bi}}''$, $\psi_{3,\mathrm{Di}}'$, and $\psi_{3,\mathrm{Di}}''$. Using these measurable parameters and equations analogous to (9) and (10), optical dynamic moduli, $G_{\mathrm{Bi}}^*(\omega)$ and $G_{\mathrm{Di}}^*(\omega)$, may be calculated. It will prove to be convenient to define G_{Bi}^* and G_{Di}^* such that their relationships to the corresponding optical ψ_3^* coefficients do not depend on the factor $1/\alpha$:

$$G_{\mathrm{Bi}}^*(\omega) = -\sum_{m=0}^{\infty}\frac{1}{2^m}[(2^m\omega)^2\psi_{3,\mathrm{Bi}}^*(2^m\omega)] \quad (13)$$

$$G_{\mathrm{Di}}^*(\omega) = -\sum_{m=0}^{\infty}\frac{1}{2^m}[(2^m\omega)^2\psi_{3,\mathrm{Di}}^*(2^m\omega)] \quad (14)$$

We shall see below that the stress and complex refractive index tensors are fundamentally related to the orientation distribution of polymer segments.[3] However, Doi et al.[22] have shown that the stress tensor of polymer melts in their terminal and plateau zones (on time scales beyond the Rouse relaxation time of an entanglement strand) is determined by orientation at the length scale of chain entanglements, whereas the individual bond orientations determine the complex refractive index tensor. Each orientation distribution is described by an order parameter, and the two order parameters are related through an orientational coupling coefficient ϵ. Since the strength (and even the existence) of orientation coupling is not known *a priori* for miscible blends, we make the simplest possible assumption for the remainder of this section, that the orientational coupling is negligible ($\epsilon = 0$). This assumption means that the order parameters for the stress and complex refractive index tensors are identical. In the subsequent section (2.3) we present the more general treatment, incorporating the effects of orientational coupling. Both approaches will then be applied to the experimental data, demonstrating conclusively that orientational coupling is important for our miscible blend.

The orientations of the entanglement strands (of length r) are modeled by the vectors r_i, having an orientation distribution characterized by the order parameter $\langle r_i r_j/r^2 - {}^1/_3\delta_{ij}\rangle$. For a melt of a single polymer species the deviatoric part of the stress tensor is related to this orientation distribution by[3]

$$\sigma_{ij} = 3k_bTc_s\left\langle\frac{r_ir_j}{r^2} - \frac{1}{3}\delta_{ij}\right\rangle \quad (15)$$

where k_b is the Boltzmann constant, T is absolute temperature, and c_s is the number of strands of length r per unit volume. For convenience, we define the parameter $G_s \equiv 3k_bTc_s$, which is a material-dependent coefficient. In the homopolymer, n_{ij}' may be related to $\langle r_ir_j/r^2 - {}^1/_3\delta_{ij}\rangle$ through a coefficient we will refer to as Λ:

$$n_{ij}' = \Lambda\left\langle \frac{r_ir_j}{r^2} - \frac{1}{3}\delta_{ij} \right\rangle \tag{16}$$

and likewise, n_{ij}'' is proportional to $\langle r_ir_j/r^2 - {}^1/_3\delta_{ij}\rangle$, but through a unique coefficient, Λ^{Di}:[23]

$$n_{ij}'' = \Lambda^{Di}\left\langle \frac{r_ir_j}{r^2} - \frac{1}{3}\delta_{ij} \right\rangle \tag{17}$$

For birefringence, Kuhn analysis[3] leads to an expression for Λ in terms of the real part of the isotropic (average) refractive index and the difference in the polarizabilities parallel and perpendicular to the segment. Combining (15) and (16) yields the familiar stress-optic rule: $n_{ij}' = C\sigma_{ij}$, where $C = \Lambda/G_s$ is the stress-optic coefficient. Similarly, combination of (15) and (17) produces a dichroism stress-optic rule with a dichroism stress-optic coefficient, $C^{Di} = \Lambda^{Di}/G_s$. In terms of the dynamic modulus, the stress-optic rule dictates that for a (dichroic) homopolymer melt $G_{Bi}^* = cG^*$ and $G_{Di}^* = c^{Di}G^*$, where $c = C\alpha$ and $c^{Di} = C^{Di}\alpha$. Note that the stress-optic coefficient and parameter α are lumped into a single coefficient due to the choice of definition for G_{Bi}^* and G_{Di}^*, alleviating the need to explicitly determine both α and C (or C^{Di}, as the case may be). The modified stress-optic coefficients, c and C^{Di}, may be experimentally determined for a given homopolymer from the ratios of G_{Bi}^* to G^* and G_{Di}^* to G^*, respectively.

As pointed out in the Introduction, for a miscible blend of polymers A and B the total stress is the sum of the stress experienced by each component. For birefringence, application of the stress-optic rule to (2) gives

$$G_{Bi}^* = c_AG_A^* + c_BG_B^* \tag{18}$$

where typically $c_A \neq c_B$. In general, c_A and c_B may be functions of blend composition; however, given that the blend components studied here are comprised of similar chemical units and that these species do not exhibit specific interactions, the composition dependence of the stress-optic coefficients is expected to be negligible. Indeed, the combined results of the birefringence, dichroism, and stress measurements in the blends discussed below support this assumption.

By focusing on a wavelength at which only one component absorbs the transmitted beam, dichroism may be used as a means of isolating that component's orientation. In the technique described here, deuterium labeling provides one component with the necessary distinct absorption behavior (specifically an absorption peak at the wavelength associated with the carbon–deuterium stretching vibration). For a blend in which a fraction of the component A chains are replaced by the deuterated counterpart, the dichroism stress-optic rule dictates

$$G_{Di}^* = f_A^{deut}c_A^{Di}G_A^* \tag{19}$$

where f_A^{deut} is the fraction of A chains in the blend which have been deuterated ($\phi_A^{deut} = f_A^{deut}\phi_A$). Like the birefringence stress-optic coefficients, c_A^{Di} is expected to be independent of blend composition.

With knowledge of the stress-optic coefficients (from optical and mechanical measurements on the pure components) and with experimentally acquired G^*, G_{Bi}^* and G_{Di}^*, expressions 2, 18, and 19 form a system of three equations in two unknowns (G_A^* and G_B^*), making the desired separation of G^* into constituent contributions possible using any two of the experimental observables (provided that $c_A \neq c_B$). Having the extra observable provides a means of varifying that the stress-optic coefficients are not ϕ-dependent. Again, it is emphasized that this approach assumes that birefringence and dichroism can be treated as measures of orientation at the entanglement strand level. We release this assumption in the next section by including orientational coupling.

2.3. Incorporating Orientational Coupling Effects. If orientation on the local (i.e., chemical bond) level differs appreciably from that on the entanglement strand level, analysis of the birefringence and dichroism must be modified in order for the calculated component G^* responses to reflect the state of stress experienced by each of the components.[22] A number of experiments on a variety of systems (see ref 24 and references therein) indicate that an enhancement of orientation on the local level relative to that on the entanglement strand level does, in fact, occur. This local enhancement effect is correlated to the orientational order of the surrounding molecules and is referred to as orientational coupling. In a stress relaxation experiment in a blend of two components with different relaxation rates, the faster species diffuses out of its original tube into a new tube with completely random steps (that hence bear no stress). Nevertheless, if there is orientational coupling, the individual bonds will still exhibit some residual orientation caused by the coupling interaction with unrelaxed entanglement strands. On time scales between the relaxation times of the two components, the fast relaxing chains bear no stress but have an anisotropic refractive index tensor due to orientational coupling to the slower relaxing species. Although the current view is that orientational coupling does not contribute to stress, birefringence and dichroism are affected since they are sensitive to actual bond orientations.[22] Systems which have been reported to exhibit orientational coupling include polymers swollen with different small anisotropic molecules,[25-27] bidisperse homopolymer melts,[28,29] polymer matrices containing oligomers of the same species,[24] cross-linked and un-cross-linked networks swollen with high polymers of a compatible species,[30,31] and monodisperse homopolymer melts having labeled center or end segments.[32] Thus, it is reasonable to expect orientational coupling to arise in high molecular weight blends of dissimilar polymers.

The contribution of orientational coupling between a given probe species and its surroundings is modeled by a simple proportionality rule:[22,28]

$$\langle u_iu_j\rangle_{probe} = \epsilon\langle u_iu_j\rangle_{bulk} \tag{20}$$

where the unit vectors u_i describe the local orientation of the freely jointed (Kuhn) bonds. The coupling coefficient ϵ depends on the nature of the probe as well as the bulk and has a physically meaningful range of $0 \leq \epsilon \leq 1$. The overall orientational order parameter at the local level is the sum of the contributions from orientational coupling and from strain-induced order on the entanglement strand level (normalized to account for the difference in length scales). For the case of a homopolymer (where probe and bulk are one in the same) this leads to the following relationship between orientational order at the two length scales:[22,28]

$$\left\langle u_i u_j - \frac{1}{3}\delta_{ij} \right\rangle = \left(\frac{1}{1-\epsilon}\right)\frac{3r^2}{5n^2b^2}\left\langle \frac{r_i r_j}{r^2} - \frac{1}{3}\delta_{ij} \right\rangle \quad (21)$$

where n is the number of bonds of length b per entanglement strand. For convenience we define the material-dependent parameter $k \equiv 3r^2/(5n^2b^2)$. From this expression, it can be seen that the presence of orientational coupling effectively influences birefringence, dichroism, and the stress-optic rule for a single-component system *only* in the values of the proportionality constants. Specifically, in light of (21), expressions 16 and 17, relating n_{ij}' and n_{ij}'' to $\langle r_i r_j/r^2 - {}^1/_3\delta_{ij}\rangle$, bear an implicit dependence on ϵ through a multiplicative factor of $1/(1-\epsilon)$ embedded in the coefficients Λ and Λ^{Di} (since the left-hand sides of (16) and (17) are actually governed by $\langle u_i u_j - {}^1/_3\delta_{ij}\rangle$). Likewise, the factor $1/(1-\epsilon)$ is then also embodied in c and c^{Di} of the stress-optic relationships. For a dichroic homopolymer n_{ij} may now be expressed in terms of either local order or entanglement strand order as follows:

$$n_{ij}' = \Lambda\left\langle \frac{r_i r_j}{r^2} - \frac{1}{3}\delta_{ij} \right\rangle = \frac{\Lambda^\circ}{k}\left\langle u_i u_j - \frac{1}{3}\delta_{ij} \right\rangle \quad (22)$$

$$n_{ij}'' = \Lambda^{Di}\left\langle \frac{r_i r_j}{r^2} - \frac{1}{3}\delta_{ij} \right\rangle = \frac{\Lambda^{\circ Di}}{k}\left\langle u_i u_j - \frac{1}{3}\delta_{ij} \right\rangle \quad (23)$$

where Λ and Λ^{Di} and ϵ-dependent, but $\Lambda^\circ = (1-\epsilon)\Lambda$ and $\Lambda^{\circ Di} = (1-\epsilon)\Lambda^{Di}$ are *not*.

For miscible blends the corresponding counterparts to (21)–(23) take on slightly more complicated forms due to coupling between chains of the different species as well as between chains of the same species. Following the Doi approach[22] used to derive (21), local orientation for each species is given by

$$\left\langle u_i u_j - \frac{1}{3}\delta_{ij} \right\rangle_A = k_A\left\langle \frac{r_i r_j}{r^2} - \frac{1}{3}\delta_{ij} \right\rangle_A + \phi_A\epsilon_{AA}\left\langle u_i u_j - \frac{1}{3}\delta_{ij} \right\rangle_A + \phi_B\left(\frac{c_{s,B}n_B}{c_{s,A}n_A}\right)\epsilon_{AB}\left\langle u_i u_j - \frac{1}{3}\delta_{ij} \right\rangle_B \quad (24)$$

$$\left\langle u_i u_j - \frac{1}{3}\delta_{ij} \right\rangle_B = k_B\left\langle \frac{r_i r_j}{r^2} - \frac{1}{3}\delta_{ij} \right\rangle_B + \phi_B\epsilon_{BB}\left\langle u_i u_j - \frac{1}{3}\delta_{ij} \right\rangle_B + \phi_A\left(\frac{c_{s,A}n_A}{c_{s,B}n_B}\right)\epsilon_{BA}\left\langle u_i u_j - \frac{1}{3}\delta_{ij} \right\rangle_A \quad (25)$$

where $c_{s,i}$ is the number of component i entanglement strands per unit volume (in the pure state) and n_i is the number of freely jointed bonds per i entanglement strand.

On the right-hand side of (24), the first term is the contribution associated with the strain-induced orientation of A chain entanglement strands, the second term is due to orientation coupling of A chains with other A chains (characterized by the scalar coupling coefficient ϵ_{AA}), and the third term accounts for orientational coupling of A chains with B chains (characterized by ϵ_{AB}). The factor $(c_{s,B}n_B/c_{s,A}n_A)$ in the third term is the ratio of the number of local segments, or bonds, per unit volume for the two species in their pure state (for most systems this ratio is roughly unity). It is included because, in accord with the proposed coupling of eq 20, the contribution of the "cross"-coupling term will depend on the relative number of B *bonds* in the blend, which is not necessarily determined by the volume fraction of B chains ϕ_B alone. (This ratio does not appear in the final expressions for G_{Bi}^* and G_{Di}^* due to cancellation with other coefficients.) The terms in (25) have analogous origins as those described for (24). For generality, we proceed with the derivation treating all four ϵ values as distinct, although coupling coefficients reported in the literature for entangled polymers typically do not vary greatly with polymer species (see ref 24 and references therein).

Table 1. Molecular Weight Characterization and Microstructure of Blend Components

			microstructure (^{13}C NMR)			
polymer	M_w	M_w/M_n	% 1,2	% 1,4 *cis*	% 1,4 *trans*	% 3,4
PI	75 000	<1.1	0	76	18	6
d-PI	90 000	<1.1	0	77	17	5
1,2-PB	204 000	<1.1	>99	0	0	

From (22) and (23) and the additivity of birefringence, n_{ij}' and n_{ij}'' for a blend with deuterium-labeled A chains may be expressed as

$$n_{ij}' = \frac{\phi_A\Lambda_A^\circ}{k_A}\left\langle u_i u_j - \frac{1}{3}\delta_{ij} \right\rangle_A + \frac{\phi_B\Lambda_B^\circ}{k_B}\left\langle u_i u_j - \frac{1}{3}\delta_{ij} \right\rangle_B \quad (26)$$

$$n_{ij}'' = \frac{\phi_A^{deut}\Lambda_A^{\circ Di}}{k_A}\left\langle u_i u_j - \frac{1}{3}\delta_{ij} \right\rangle_A \quad (27)$$

Using the preceding four equations relating orientation on the two length scales and the refractive index tensor to local orientation along with application of (15), expressions for the optical G^* in terms of G_A^* and G_B^* (incorporating the effects of orientational coupling) may now be derived:

$$G_{Bi}^* = c_A^\circ\left[\frac{G_A^* + \frac{\phi_A}{\phi_B}\left(\frac{\phi_B\epsilon_{AB}}{1-\phi_B\epsilon_{BB}}\right)G_B^*}{(1-\phi_A\epsilon_{AA}) - \left(\frac{\phi_B\epsilon_{AB}}{1-\phi_B\epsilon_{BB}}\right)\phi_A\epsilon_{BA}}\right] + c_B^\circ\left[\frac{G_B^* + \frac{\phi_B}{\phi_A}\left(\frac{\phi_A\epsilon_{BA}}{1-\phi_A\epsilon_{AA}}\right)G_A^*}{(1-\phi_B\epsilon_{BB}) - \left(\frac{\phi_A\epsilon_{BA}}{1-\phi_A\epsilon_{AA}}\right)\phi_B\epsilon_{AB}}\right] \quad (28)$$

$$G_{Di}^* = f_A^{deut}c_A^{\circ Di}\left[\frac{G_A^* + \frac{\phi_A}{\phi_B}\left(\frac{\phi_B\epsilon_{AB}}{1-\phi_B\epsilon_{BB}}\right)G_B^*}{(1-\phi_A\epsilon_{AA}) - \left(\frac{\phi_B\epsilon_{AB}}{1-\phi_B\epsilon_{BB}}\right)\phi_A\epsilon_{BA}}\right] \quad (29)$$

where $c_i^\circ = (1-\epsilon_{ii})c_i$. Note that in the limit of all $\epsilon = 0$ these equations reduce to (18) and (19). Once the stress-optic coefficients are determined from optical and mechanical experiments on the pure components and the coupling coefficients are assessed, eqs 2, 28, and 29 form a new system of three equations in two unknowns, which can be used to determine G_A^* and G_B^* in a miscible polymer blend. Since the assumption that the stress-optic coefficients are composition independent is not expected to be universal for blends (particularly with birefringence), the third observable serves as an essential cross check in the current study.

3.0. Experimental Section

Blend components were prepared by anionic polymerization to achieve a narrow distribution of molecular weights. Table 1 lists the molecular weight and microstructural characteristics of

the polymers. Details regarding the synthesis and characterization of the 1,2-PB are published in ref 33.

Blends containing 20, 40, 60, and 80% by weight 1,2-PB have been studied, all of which contain 6% by weight deuterated PI. This deuterated PI content was found to yield the optimal dichroism signal-to-noise ratio for 0.5 mm thick samples. Blends were prepared by dissolving the components in cyclohexane and film casting the solutions at room temperature. To further reduce solvent content, samples were kept under vacuum at room temperature for no less than 48 h and annealed at 60 °C for an additional 24 h under vacuum. To prevent oxidation, 0.1 wt % 2,6-di-*tert*-butylcresol was added in the preparation of all samples, and prior to usage, samples were stored at 0 °C in containers flushed with nitrogen.

Mechanical oscillatory shear rheometry was conducted on the pure components and blends at temperatures well above T_g using a Rheometrics RMS-800 mechanical spectrometer with a force-rebalanced transducer. Parallel plate geometry was employed with 8 mm diameter plates and 1–2 mm gap heights over a frequency range of 0.01–100 rad/s. Temperature control was achieved by circulating heated nitrogen through the sample chamber.

Oscillatory shear IR dichroism and birefringence measurements were conducted using an apparatus whose design has been previously described.[18,28] Several modifications were implemented to meet the current experimental needs. To extend the accessible frequency range, an improved servo motor system (PMI Motions Technologies Model U9M4H motor with VXA48-8-8 amplifier) was installed. The current accessible frequency range extends from below 0.01 to 100 rad/s. Accurate sample temperature control is achieved by heating the parallel plates (CaF_2 windows) with separately controlled electric resistive heaters. The heaters are mounted in the aluminum window holders and the feedback temperature probes (type J thermocouples) are mounted directly on the window surfaces adjacent to the polymer sample. Calibration experiments indicate an accuracy of ±0.1 °C over the temperature range studied here.

Gap widths at each of the temperatures studied were calibrated using micrometer measurements of the thicknesses of unloaded samples having T_g's at or slightly above the flow cell temperature. The calibration samples (poly(ethylene oxide)/poly(methyl methacrylate) blends of varying composition) were preheated to roughly 20 °C above the flow cell temperature prior to loading in the preheated flow cell. Accuracy of the sample thicknesses is within 5%. Any systematic error in sample thickness affects the stress-optic coefficients, but it does not affect the recovery of the component G^* contributions (provided that the error in the thickness remains the same for the blends as for the pure components at a given temperature).

In previous oscillatory IR dichroism and birefringence experiments[8,18] only normalized optical measurements were reported. Calibration measurements, required to relate the optical signals to stress, may be obtained when the intensity offsets observed by each detector are measured. As discussed in ref 28, using the Mueller formalism the intensities measured by the detectors may be shown to be of the form

$$I = I_{dc} + I_f \sin(ft) + I_{2f} \cos(2ft) + \ldots \tag{30}$$

where f is the frequency of the photoelastic modulator. Of interest here are I_f^{Bi} and I_{2f}^{Di}, recovered from the detector intensities using lock-in amplifiers, along with I_{dc}^{Bi} and I_{dc}^{Di}, found using low-pass filters. Dichroism is related to the intensity ratio

$$I_{2f}^{Di}/I_{dc}^{Di} = 2J_2(A) \tanh \nu \tag{31}$$

where $J_2(A)$ is the value of the Bessel function at A, the amplitude of photoelastic modulation, and the extinction $\nu = (2\pi d/\lambda)\Delta n''$ (where d = sample thickness and λ = laser wavelength). A is chosen such that $J_0(A) = 0$, a condition required for the validity of (31). Similarly, birefringence is recovered from

$$I_f^{Bi}/I_{dc}^{Bi} = 2J_1(A)\frac{\sin \mu}{\cosh \nu} \tag{32}$$

where the retardance $\mu = (2\pi d/\lambda)\Delta n'$. $J_1(A)$ and $J_2(A)$ are experimentally determined from calibration experiments using a quarter-wave retarder or a polarizer in place of the sample.

In the dynamic optical experiments intensity measurements were made at a rate of 64 measurements per strain cycle and typically data for 5–20 strain cycles were averaged at each strain frequency. Data were collected at strain frequencies equally spaced on a logarithmic scale by an increment of log $2^{1/2}$ (approximately 7 data points per decade). Direct application of (13) and (14) to the data (without interpolation) requires a log ω increment of log 2. Twice this number of data points per strain frequency decade are collected here to gain better resolution of the G^* frequency dependence. To apply (13) and (14), the data are then alternately grouped into two sequences, each having the required log 2 increment.

The strain frequency range studied spanned from as low as 0.01 to 100 rad/s, imposing strain amplitudes of 15–30% on 0.5 mm thick samples, where the higher strains were applied at the lower frequencies (for this range of strains, μ and ν were much less than $\pi/2$). Linear viscoelasticity was verified by consistent results at strains ranging from 10 to 50%. Experiments were conducted at 21, 40, 60, 80, and 100 °C (except for pure PI, for which experiments were run at 21, 30, 40, and 50 °C due to its fast relaxation). Experiments for each set of conditions were repeated at least once to ensure reproducibility.

As described above, separation of G^* into component contributions requires two dynamic observables. In the analysis here we choose to use the two which have the strongest signal-to-noise ratio, the mechanical and birefringence results. G_{PI}^* and G_{PB}^* are then calculated from either (2) and (18) if the effects of orientational coupling are neglected or (2) and (28) if the effects of orientational coupling are to be included. In either case stress-optic coefficients recovered from pure component experiments are used, and in the latter approach reasonable estimates for the coupling coefficients must be introduced. For simplification, we neglect the possible differences that may exist between the various coupling coefficients and use a mean coupling coefficient ϵ in the calculations. As will be discussed below, from the calculated component dynamic moduli, it is possible to approximate the value of ϵ. Dichroism is used as an essential cross-check to confirm the validity of the assumption that the stress-optic coefficients do not vary with composition. This is done by comparing the measured G_{Di}^* to that predicted using (19) or (29) with the experimentally determined component contributions to G^*.

4.0. Results and Discussion

4.1. Pure Components. Before the blend dynamic moduli can be separated into component contributions, knowledge of the pure component stress-optic coefficients must be acquired. Master curves of the pure component dynamic moduli were constructed based on the time–temperature superposition principle:[1]

$$G^*(\omega;T) = b_T G^*(a_T\omega;T_0) \tag{33}$$

which relates the dynamic modulus at temperature T to that at a reference temperature T_0 through a modulus shift factor b_T and frequency shift factor a_T, which are temperature dependent (but frequency independent) material parameters. These shift factors serve as measures of the temperature dependences of the plateau modulus and relaxation time of the material. Master curves constructed from both optical and mechanical results are presented in Figure 2. In generating these master curves, the optical moduli at different temperatures were first determined from the raw daw and then superimposed. Each of the graphs in this figure shows a given optical modulus plotted with the mechanical modulus for the same component on scales appropriate for comparison. Good time–temperature superposition for all signals is observed. Moreover, there is good agreement between the mechanical and optical moduli in general, supporting the validity of the constitutive relationships and stress-optic rule for the polymers studied here. Notice, however, that a significant deviation between the optical and mechanical moduli arises

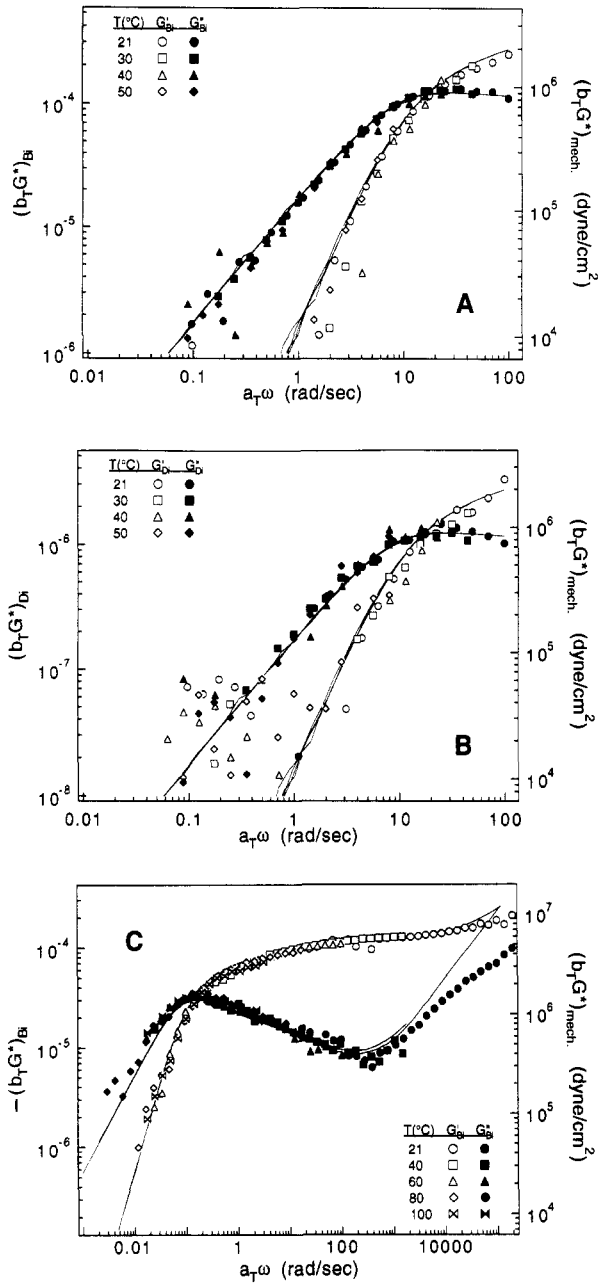

Figure 2. Master curves of the mechanically and optically measured $G^*(\omega)$ for pure components. Mechanical data are represented by the solid lines and optical data are denoted by symbols: (A) G_{Bi}^* and G^* for pure PI, referenced to $T_0 = 21$ °C; (B) G_{Di}^* and G^* for pure PI, referenced to $T_0 = 21$ °C; (C) $-G_{Bi}^*$ and G^* for pure 1,2-PB, referenced to $T_0 = 60$ °C. Note that negative birefringence results are plotted for 1,2-PB.

at high frequencies for 1,2-PB, coincident with the rubber-to-glass transition (Figure 2C). This failure of the stress-optic rule is attributed to the additional contribution of glassy stress relaxation modes at such high frequencies (short time scales).[34] Similar observations have been previously reported and more thoroughly investigated by Read studying poly(methyl acrylate)[34] and Inoue et al. studying polystyrene.[35] In both of those studies, the onset of glassy behavior was found to induce positive deviations from the stress-optic coefficient, as observed here. The failure of the stress-optic rule in the transition regime limits the applicability of the method to the rubbery plateau and terminal relaxation regions in the blends, but these regions are generally of greatest interest and so the restriction is not overly confining.

Further support for the method relating the optical measurements to mechanical ones is provided by the excellent agreement between the optical and mechanical

Table 2. Stress-Optic Coefficients and Shift Factors for Pure Components

polymer	T (°C)	a_T	b_T	$a_{T,Bi}$	$a_{T,Di}$	c (cm²/dyn)[a]	c^{Di} (cm²/dyn)[a]
PI	21	1	1	1	1	$1.3_8 \times 10^{-10}$	2.3×10^{-11}
PI	30	0.47	1.09	0.46	0.46	$1.2_8 \times 10^{-10}$	2.1×10^{-11}
PI	40	0.225	1.18	0.23	0.23	$1.2_1 \times 10^{-10}$	2.0×10^{-11}
PI	50	0.12	1.24	0.11	0.11	$1.1_4 \times 10^{-10}$	1.9×10^{-11}
1,2-PB	21	1200	1.02	1100		$-3.1_5 \times 10^{-11}$	
1,2-PB	40	18	1.01	17		$-2.8_6 \times 10^{-11}$	
1,2-PB	60	1	1	1		$-2.5_4 \times 10^{-11}$	
1,2-PB	80	0.16	0.97	0.17		$-2.2_8 \times 10^{-11}$	
1,2-PB	100	0.033	0.97	0.032		$-2.1_3 \times 10^{-11}$	

[a] c and c^{Di} contain the factor α.

frequency shift factors a_T (Table 2). With the exceptions of the lowest temperature for 1,2-PB (where the transition to glassy behavior dominates) and the highest temperature for PI (where the optical signals are weak), the shift factors are virtually identical. Based on these observations, we conclude that the method for relating dynamic 1,3-birefringence and dichroism to G^* outlined above is valid for the pure component polymer melts considered here. To the best of our knowledge, this is the first time these optical anisotropies have been utilized to determine the dynamic modulus.

Mean values for the ratios of the optical and mechanical $|G^*|$ give the stress-optic coefficients c and c^{Di} at each temperature, which are reported in Table 2 (recall that these coefficients embody the factor $\alpha = N_3/N_1$). Due to the scatter in the optical results at low frequencies, calculation of the stress-optical coefficients were made using optical data spanning roughly from the maximum signal down to about 10% of the maximum. Standard deviations for the birefringence stress-optic coefficients were about 5% for PI and 3% for 1,2-PB, and the standard deviation for the PI dichroism stress-optic coefficient was about 10%. Values of C_{PI} are available in the literature for comparison; however, discretion must be exercised in making such a comparison (even if the α factor is accounted for) since stress-optic coefficients tend to be mildly wavelength dependent and the literature values correspond to $\lambda = 632$ nm. With this in mind, we assumed $\alpha \equiv 1 + N_2/N_1 = 0.76$, based on results reported for PI melts,[19] and calculate $C_{PI} = 1.8 \times 10^{-10}$ cm²/dyn at room temperature, which does not differ significantly from literature values (1.9×10^{-10} cm²/dyn).[19,36] The fact that c_{PI}^{Di} is an order of magnitude smaller than c_{PI} is consistent with observations on poly(ethylenepropylene) melts[28] and is partly responsible for the poorer dichroism signal-to-noise ratio evident in Figure 2B (the low volume fraction of deuterated component also plays a role). The negative stress-optic coefficient for 1,2-PB and its smaller magnitude are in agreement with behavior observed in similar vinyl polymers.[16,37] The fact that c_{PI} and c_{PB} are of opposite sign facilitates the identification of each component's contribution to birefringence in the blend. In accord with Kuhn–Grun theory,[16] the stress-optic coefficients appear to be inversely proportional to the absolute temperature, although the data admittedly span only a limited temperature range.

4.2. Blends. Initial analysis of the blend dynamic moduli is conducted assuming the effects of orientational coupling can be neglected. Figure 3 depicts a typical example of the calculated component dynamic moduli obtained from mechanical and birefringence measurements using (2) and (18) (or equivalently (2) and (28) with $\epsilon = 0$). From the recovered G_{PI}^* response, a prediction for the dichroism response can be calculated using (19) (or equivalently (29) with $\epsilon = 0$) to test the composition

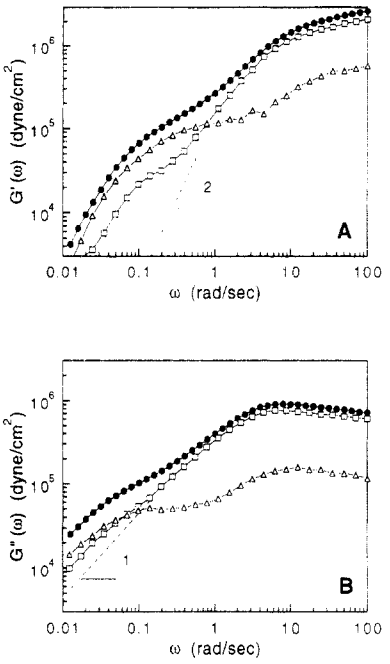

Figure 3. Dynamic modulus (●) and component contributions (□ = G_{PI}*, △ = G_{PB}*) for the 20% 1,2-PB blend at 21 °C: (A) storage moduli; (B) loss moduli. Component G* were computed from mechanical and birefringence measurements using (2) and (18). The dashed curves provide a qualitative comparison to the terminal response of a polymer liquid.

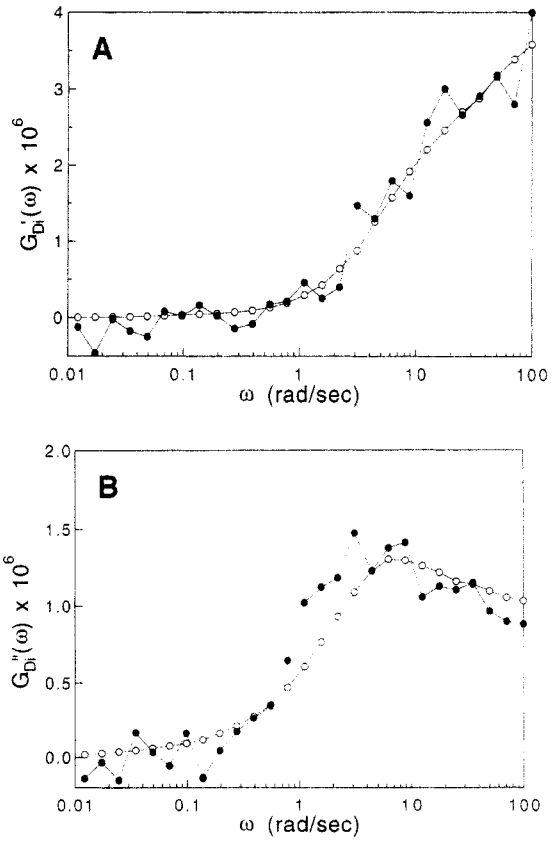

Figure 4. Comparison of measured dichroism to that calculated based on the recovered component G* for 20% 1,2-PB at 21 °C: (A) G_{Di}'; (B) G_{Di}''. Solid symbols (●) correspond to the measured dichroism response and hollow ones (○) to the calculated dichroism response.

independence of the stress-optic coefficients. These results are compared to the measured dichroism response in Figure 4. If the stress-optic coefficients indeed vary with blend composition, poor comparison of the shapes and especially the amplitudes of the calculated and measured dichroism signals would be expected. To the contrary, the current

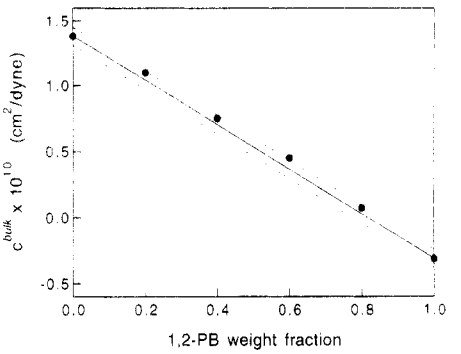

Figure 5. Composition dependence of the bulk stress-optic coefficient at 21 °C. Error bars are based on the uncertainty in the pure components.

results show good agreement. Such agreement is observed at all compositions and temperatures. The good agreement between the calculated and measured dichroism response is strong evidence that the component stress-optic coefficients are independent of composition in this blend. Strictly speaking, due to the variability in the data, it is not possible to rule out the occurrence of small deviations from the pure component stress-optic coefficients. Such potential variations here are estimated to be less than 5% based on the analysis of the results at different compositions and temperatures using different assumed values of the stress-optic coefficients.

Further support that the stress-optic coefficients are composition independent is offered by the composition dependence of the bulk stress-optic coefficient, c^{bulk}, computed from the ratio of the overall blend $|G_{Bi}^*|$ to the mechanically acquired $|G^*|$. In the blends this ratio is not a constant but rather varies with shear frequency due to the differing relaxation times of the two components. However, at high frequencies as the rubbery plateau of each component is approached, a frequency-independent c^{bulk} value is approached. In this high-frequency limit, we monitor the composition dependence of c^{bulk}. The results from experiments at 21 °C are plotted in Figure 5. The near linearity of the plot gives additional confidence that the component stress-optic coefficients are invariant with blend composition.

Having established confidence in the assumptions required to separate G* into component contributions, it is worth examining the features of the calculated G* contributions in Figure 3, looking in particular for evidence of orientational coupling. Interestingly, both component responses deviate significantly from normal monodisperse homopolymer behavior. In describing this unusual behavior, it is useful to note that at a given $T - T_g$ pure PI relaxes faster than pure 1,2-PB for the molecular weights studied here. Thus, in the blend it is expected that PI relaxation is primarily responsible for the G* features at higher frequencies (shorter time scales), while those at low frequencies are primarily due to 1,2-PB relaxation. Focusing on PI, it is apparent that both G_{PI}' and G_{PI}'' differ from monodisperse homopolymer behavior in the terminal zone, where both responses show positive deviations from the expected terminal scalings: $G' \sim \omega^2$ and $G'' \sim \omega$ as $\omega \to 0$. On the other hand, deviations in the 1,2-PB dynamic modulus arise at high frequency in the rubbery plateau. With increasing ω, G_{PB}' approaches a plateau as expected but then increases to a new pseudoequilibrium value at higher ω. Similarly, with increasing ω, G_{PB}'' appears to approach a local maximum at low ω but then increases to pass through a maximum at a higher frequency.

For both components the deviations are clearly correlated with the relaxation of the other component, though

for different reasons. For 1,2-PB the variation in modulus amplitude is primarily linked to the number of effective chain entanglements experienced by the 1,2-PB chains on different time scales. On a short time scale (high ω), motion of the 1,2-PB chains is restricted by entanglements with PI chains as well as other 1,2-PB chains. Broadly speaking, on a time scale intermediate to the relaxation times of PI and 1,2-PB, the PI chains have undergone stress relaxation, and consequently, 1,2-PB chain relaxation is effectively inhibited only by other 1,2-PB chains. According to rubber elasticity theory, the modulus amplitude is directly proportional to the entanglement density. Thus, as the 1,2-PB chains experience a reduction of effective entanglements (due to PI relaxation) in passing from high ω to lower ω, the 1,2-PB dynamic modulus is expected to decrease, as observed. A more detailed analysis of this constraint release effect and its composition dependence is discussed in a separate report.[15]

In contrast, the PI behavior at low ω is not related to constraint release, but rather it is an indication of orientational coupling influencing the birefringence measurements used to construct the component G^*. On a time scale greater than the PI relaxation time, the essentially stress-free PI chains find themselves in a matrix of oriented, slower relaxing 1,2-PB chains. As a result, on the local length scale, the PI chains exhibit some orientation until the 1,2-PB chains relax. As discussed above, while orientational coupling contributes to the birefringence, it does not affect stress. Thus, to acquire the actual component stress contributions, the effects of orientational coupling must be accounted for as in (28) and (29). In accounting for orientational coupling, we assume the effect can be adequately characterized by a single, composition-independent coupling coefficient $\epsilon = \epsilon_{PI-PI} = \epsilon_{PI-PB} = \epsilon_{PB-PI} = \epsilon_{PB-PB}$. To make a reasonable estimate for ϵ, we vary its value in (28) and study the effect on the component G^*, particularly in the terminal region of G_{PI}^*. Manipulation of ϵ is found to most strongly influence the shape of the PI modulus at low ω. Incorporating values of ϵ from about 0.3 to 0.4 tend to result in terminal G_{PI}^* behavior consistent with expectation (i.e., $G' \sim \omega^2$ and $G'' \sim \omega$ as $\omega \rightarrow 0$) at all compositions and temperatures studied. Thus, by application of this additional physical restriction, it is estimated that the coupling coefficient for this blend system is $\epsilon = 0.35 \pm 0.05$. The apparent insensitivity to temperature observed here is in agreement with other orientational coupling studies,[24,38] indicating an entropic origin of the coupling effect. Figures 6 and 7 depict the component loss and storage moduli at different blend compositions using $\epsilon = 0.35$. For comparison, moduli computed with $\epsilon = 0$ are also shown.

The uncertainty in the component moduli is rather small, typically less than 10%, except for PI at very low frequencies. The primary source of error is the uncertainty in the stress-optic coefficients, which was assessed by performing the analysis using the mean stress-optic coefficient plus the standard deviation for one component and the mean minus the standard deviation for the other, the vice versa. It should be noted that modest errors associated with the stress-optic coefficients do not greatly affect the shapes of the recovered moduli. Rather, they tend to shift the curves nearly uniformly on the modulus scale. The uncertainty estimate is based on values of ϵ which yield physical results (i.e., $\epsilon = 0.35 \pm 0.05$).

A natural consequence of the method for calculating component contributions is that scatter in each component modulus is some sort of weighted average of the scatter in the raw birefringence and scatter in the raw mechanical results (small by comparison). As a result, the component moduli have less noise than the raw birefringence but more than the raw mechanical results.

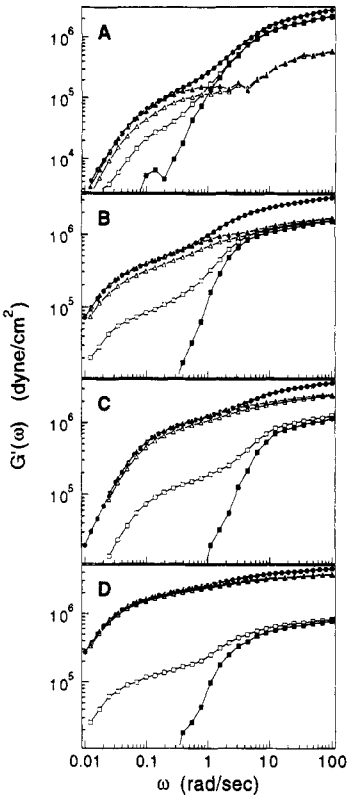

Figure 6. Blend and component storage moduli: (A) 20% 1,2-PB at 21 °C; (B) 40% 1,2-PB at 21 °C; (C) 60% 1,2-PB at 40 °C; (D) 80% 1,2-PB at 40 °C. Symbols correspond to (●) mechanically acquired G', (■) G_{PI}' using $\epsilon = 0.35$, (▲) G_{PB}' using $\epsilon = 0.35$, (□) G_{PI}' using $\epsilon = 0$, and (△) G_{PB}' using $\epsilon = 0$.

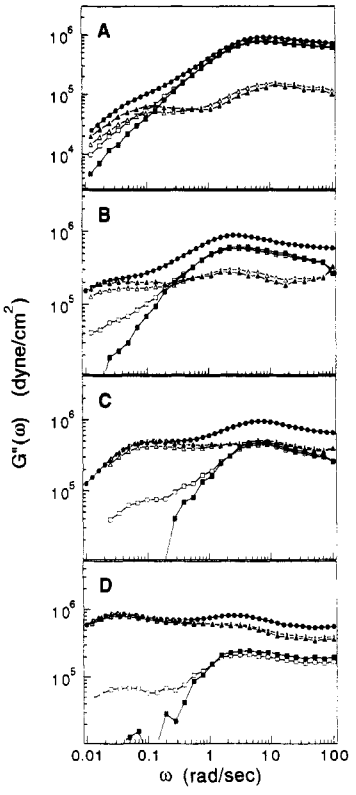

Figure 7. Blend and component loss moduli: (A) 20% 1,2-PB at 21 °C; (B) 40% 1,2-PB at 21 °C; (C) 60% 1,2-PB at 40 °C; (D) 80% 1,2-PB at 40 °C. Symbols correspond to (●) mechanically acquired G'', (■) G_{PI}'' using $\epsilon = 0.35$, (▲) G_{PB}'' using $\epsilon = 0.35$, (□) G_{PI}'' using $\epsilon = 0$, and (△) G_{PB}'' using $\epsilon = 0$.

It is worth pointing out that assessing orientational coupling as described above essentially focuses on coupling between PI chains and oriented 1,2-PB chains (i.e., ϵ_{PI-PB}).

If the various coupling coefficients actually take on differing values, ϵ_{PI-PB} is likely to represent an intermediate value (with ϵ_{PI-PI} and ϵ_{PB-PB} being the extrema). Given the small effect on the component G^* which varying ϵ has outside the terminal PI region, moderate differences in the various ϵ values would not introduce an appreciable effect on the results. Thus, a single value of $\epsilon = 0.35$ appears to be adequate for the purposes of recovering component G^* contributions in the PI/1,2-PB blend system. Again, it is emphasized that due to the existence of orientational coupling in the current system, for the calculated G^* contributions to reflect strictly the state of stress experienced by each component (and be free of contributions associated with orientational coupling on the local level), the extended approach with $\epsilon = 0.35 \pm 0.05$ must be implemented.

This value for the coupling coefficient compares rather well with reports in the literature. In highly entangled homopolymer melts a coupling coefficient of $\epsilon = 0.3$–0.45 was found for poly(ethylenepropylene)[28,29,32] and $\epsilon = 0.4$ was reported for 1,4-polybutadiene.[24,32] Zemel and Roland[30] recently measured the coupling coefficient in cross-linked networks of PI swollen with high molecular weight 1,2-PB. Large deformations were employed in that study, causing strain-induced crystallization of the PI matrix, an effect not present in the current study due to the small deformations applied. The most appropriate system in that study to compare against the current findings corresponds to their most lightly cross-linked PI network, which most closely approximates the melt, and their lower molecular weight 1,2-PB, which was found to be less sensitive to PI crystallization effects. For that system Zemel and Roland observed $\epsilon_{PB-PI} = 0.22$. Kawabata and co-workers[31] studied the orientation of poly(2,6-dimethyl-1,4-phenylene oxide) (PPO) chains of varying length in high molecular weight cross-linked and un-cross-linked polystyrene (PS). They observed a coupling coefficient of $\epsilon_{PPO-PS} \approx 0.4$ for entangled PPO chains, a value consistent with a packing entropy theory proposed by the same authors.[39] Based on these reports, our value of $\epsilon = 0.35 \pm 0.05$ seems to be reasonable for a highly entangled system.

5.0. Summary

We have described a method for the separation of the dynamic modulus of a homogeneous multicomponent polymer system into component contributions based on complementary rheo-optical and mechanical rheometry measurements. The stress-optic rule and constitutive equations applicable to polymer melts in the limit of linear viscoelasticity have been shown to successfully relate IR 1,3-dichroism and birefringence results to the mechanical dynamic modulus. Exploiting these relationships and accounting for orientational coupling permit the resolution of the complex modulus of each component in the blend. Application of the technique to miscible blends of polyisoprene and 1,2-polybutadiene demonstrates its validity and reveals the occurrence of orientational coupling in this blend, characterized by a coupling coefficient $\epsilon = 0.35 \pm 0.05$, comparable to that observed in other highly entangled systems. The outlined complementary rheo-optical/mechanical rheometry technique offers a powerful tool for probing the dynamics of multicomponent polymer systems in that it enables the effects of blending on the rheology of the individual components to be resolved. A detailed investigation of how the relaxation dynamics of each component in the PI/1,2-PB blend system are influenced by blend composition is presented in the companion paper.[15]

Acknowledgment. We are thankful for the financial support provided by Eastman Kodak Co., the National Science Foundation (Grant DMR 9120360), and the Center for Materials Research at Stanford University.

References and Notes

(1) Ferry, J. D. *Viscoelastic Properties of Polymers*, 3rd ed.; Wiley: New York, 1980.
(2) Bird, R. B.; Armstrong, R. C.; Hassager, O. *Dynamics of Polymeric Liquids*, 2nd ed.; Wiley: New York, 1987; Vol. 1.
(3) Doi, M.; Edwards, S. F. *The Theory of Polymer Dynamics*; Oxford University Press: Oxford, 1986.
(4) Montfort, J. P.; Marin, G.; Monge, P. *Macromolecules* **1984**, *17*, 1551.
(5) Watanabe, H.; Kotaka, T. *Macromolecules* **1984**, *17*, 2316.
(6) Watanabe, H.; Sakamoto, T.; Kotaka, T. *Macromolecules* **1985**, *18*, 1008.
(7) Struglinski, M. J.; Graessley, W. W. *Macromolceules* **1985**, *18*, 2630.
(8) Kornfield, J. A.; Fuller, G. G.; Pearson, D. S. *Macromolecules* **1991**, *24*, 5429.
(9) Osaki, K.; Takatori, E.; Kurata, M.; Ohnuma, H.; Kotaka, T. *Polym. J.* **1986**, *18*, 947.
(10) Osaki, K.; Takatori, E.; Ueda, M.; Kurata, M.; Kotaka, T.; Ohnuma, H. *Macromolecules* **1989**, *22*, 2457.
(11) Bouton, C.; Arrondel, V.; Rey, V.; Sergot, Ph.; Manguin, J. L.; Jasse, B.; Monnerie, L. *Polymer* **1989**, *30*, 1414.
(12) Zhao, Y.; Jasse, B.; Monnerie, L. *Polymer* **1989**, *30*, 1643.
(13) Roland, C. M. *J. Polym. Sci., Polym. Phys. Ed.* **1988**, *26*, 839.
(14) Tomlin, D. W.; Roland, C. M. *Macromolecules* **1992**, *25*, 2994.
(15) Zawada, J. A.; Fuller, G. G.; Colby, R. H.; Fetters, L. J.; Roovers, J. *Macromolecules*, following paper in this issue.
(16) Janeschitz-Kriegl, H. *Polymer Melt Rheology and Flow Birefringence*; Springer-Verlag: New York, 1983.
(17) Gao, H. W.; Ramachandran, S.; Christiansen, E. B. *J. Rheol.* **1981**, *25*, 213.
(18) Kornfield, J. A.; Fuller, G. G.; Pearson, D. S. *Rheol. Acta* **1990**, *29*, 105.
(19) Kannan, R. M.; Kornfield, J. A. *Rheol. Acta* **1992**, *31*, 535.
(20) Osaki, K.; Kimura, S.; Kurata, M. *J. Polym. Sci., Polym. Phys. Ed.* **1981**, *19*, 517.
(21) Meissner, J.; Garbella, R. W.; Hostettler, J. *J. Rheol.* **1989**, *33*, 843.
(22) Doi, M.; Pearson, D.; Kornfield, J.; Fuller, G. *Macromolecules* **1989**, *22*, 1488.
(23) Michl, J.; Thulstrup, E. W. *Spectroscopy with Polarized Light*; VCH: New York, 1986.
(24) Ylitalo, C. M.; Zawada, J. A.; Fuller, G. G.; Abetz, V.; Stadler, R. *Polymer* **1992**, *33*, 2949.
(25) Deloche, B.; Samulski, E. T. *Macromolecules* **1981**, *14*, 575.
(26) Thulstrup, E. W.; Michl, J. *J. Am. Chem. Soc.* **1982**, *104*, 5594.
(27) Schmidt, P.; Schneider, B. *Makromol. Chem.* **1983**, *184*, 2075.
(28) Kornfield, J. A.; Fuller, G. G.; Pearson, D. S. *Macromolecules* **1989**, *22*, 1334.
(29) Ylitalo, C. M.; Kornfield, J. A.; Fuller, G. G.; Pearson, D. S. *Macromolecules* **1991**, *24*, 749.
(30) Zemel, I. S.; Roland, C. M. *Polymer* **1992**, *33*, 4522.
(31) Kawabata, K.; Fukuda, T.; Yoshinobu, T.; Miyamoto, T. *Macromolecules* **1993**, *26*, 3980.
(32) Ylitalo, C. M.; Fuller, G. G.; Abetz, V.; Stadler, R.; Pearson, D. S. *Rheol. Acta* **1990**, *29*, 543.
(33) Roovers, J.; Toporowski, P. M. *Rubber Chem. Technol.* **1990**, *63*, 734.
(34) Read, B. E. *Polymer* **1964**, *5*, 1.
(35) Inoue, T.; Okamoto, H.; Osaki, K. *Macromolecules* **1991**, *24*, 5670.
(36) Vinogradov, G. V.; Isayev, A. I.; Mustafaev, D. A.; Podolsky, Y. Y. *J. Appl. Polym. Sci.* **1978**, *22*, 665.
(37) Brandrup, J.; Immergut, E. H. *Polymer Handbook*, 2nd ed.; Wiley: New York, 1975.
(38) Ylitalo, C. M.; Fuller, G. G. *Macromolecules* **1991**, *24*, 5736.
(39) Fukuda, T.; Kawabata, K.; Yoshinobu, T.; Miyamoto, T. *Macromolecules* **1992**, *25*, 2196.